Synthetic Metals 240 (2018) 59–66

Contents lists available at ScienceDirect

Synthetic Metals

journal homepage: www.elsevier.com/locate/synmet

Metallic conductivity beyond the Mott minimum in PEDOT: Sulphate at low temperatures

Farka Dominik[a,*], Andrew O.F. Jones[b], Reghu Menon[c], Niyazi Serdar Sariciftci[a], Philipp Stadler[a]

[a] Linz Institute for Organic Solar Cells (LIOS) Physical Chemistry, Johannes Kepler University Linz, Altenbergerstraße 69, 4040, Linz, Austria
[b] Institute of Solid State Physics, Graz University of Technology, Petersgasse 16, 8010 Graz, Austria
[c] Department of Physics, Indian Institute of Science, Bangalore 560012, India

ARTICLE INFO

Keywords:
PEDOT:sulphate
Magnetoconductivity
Metallic conductive polymer
Conductivity minimum
Pressure dependence
Mott minimum

ABSTRACT

Elastic scattering mechanisms dominate the charge transport in crystalline metals, resulting in a characteristic increase in conductivity at low temperatures. However, disorder – arising, for example, from alloying – can hamper transport and lead to decreased coherence among scattered electrons (*i.e.* inelastic scattering). This is typically the situation in non-crystalline metals. Likewise, conductive polymers are particularly prone to defect states with decreased carrier mobility (*i.e.* electrical conductivity).

We present the first report of conduction in the elastic scattering regime in conductive polymers without the detrimental effect on conductivity. As in a crystalline metal, conductivity increases upon cooling. More specifically, we observed a minimum conductivity in free-standing metallic PEDOT:sulphate at around 4 K. The polymer chains, which form crystallites of around 800 Å in size, exhibit an extraordinary degree of spatial and energetic order. We show that increasing pressure enabled us to shift the minimum upwards, thus achieving metallic conductivity at up to 10 K with a calculated mean-free path of around 250 Å. These results underline the existence of true metallic states in conductive polymers at low temperatures.

1. Introduction

Recent years have seen great advances in organic polymeric conductors. Novel materials of high purity and with low levels of disorder exhibit very high conductivities ($> 5000\ S\ cm^{-1}$) [1–3]. Nevertheless, the question remains of how to bridge the gap to true metallic conductivity, that is, how to achieve a positive temperature coefficient of resistance (TCR) as is typical of classical metals [4–9]. Conductive polymers (CPs) are different from metals, particularly in their inherent quasi-one-dimensional nature, which makes them especially prone to disorder. However, there are also similarities, for example, to alloys and amorphous metals [10–12], in which- unlike crystalline metals- conductivity does not increase with decreasing temperature [13,14].

Building on the theory of Anderson and Mott, we hypothesized that weak localization is directly linked to disorder in the system. The next step in the development of conductive polymers therefore consists of overcoming the critical density of states g* to make the transition to a metallic and – potentially – in the longer term to a superconductive system [15–21].

Fornari et al [22]. arrived at a similar conclusion, claiming that only two distinct parameters influence conductivity: the activation energy of electrical transport (which is given by the chemical structure of the molecule) and disorder. Hence, to achieve high conductivity, not only the choice of molecule is crucial, but, even more so, its processing into thin films.

Based on these conclusions, we decided to investigate the conductive material poly(3,4-ethylenedioxythiophene) (PEDOT), which is known for its structural advantages and mass production worldwide, and processed it in a novel way to minimize disorder during thin-film deposition and doping.

In this work, we investigate films of PEDOT:sulphate deposited via oxidative Chemical Vapour Deposition (oCVD). A previous publication reported that, due to an extraordinary degree of structural order, this material exhibits the hallmarks of a glassy metal [23]. Here, we present a study of bulk properties with the aim to eliminate effects related to the substrate.

We applied high pressures to compress the molecules in the van-der-Waals crystal, further suppress disorder, and thus to facilitate carrier transport [24–26] between polymer chains. Our assumption was that we could bridge the phenomenological gap between metals and conductive polymers by promoting diffusive electron motion and thus increasing the overlap between wavefunctions.

* Corresponding author.
E-mail addresses: dominik.farka@jku.at, dominik.farka@gmx.at (F. Dominik).

https://doi.org/10.1016/j.synthmet.2018.03.015
Received 29 November 2017; Received in revised form 6 March 2018; Accepted 16 March 2018

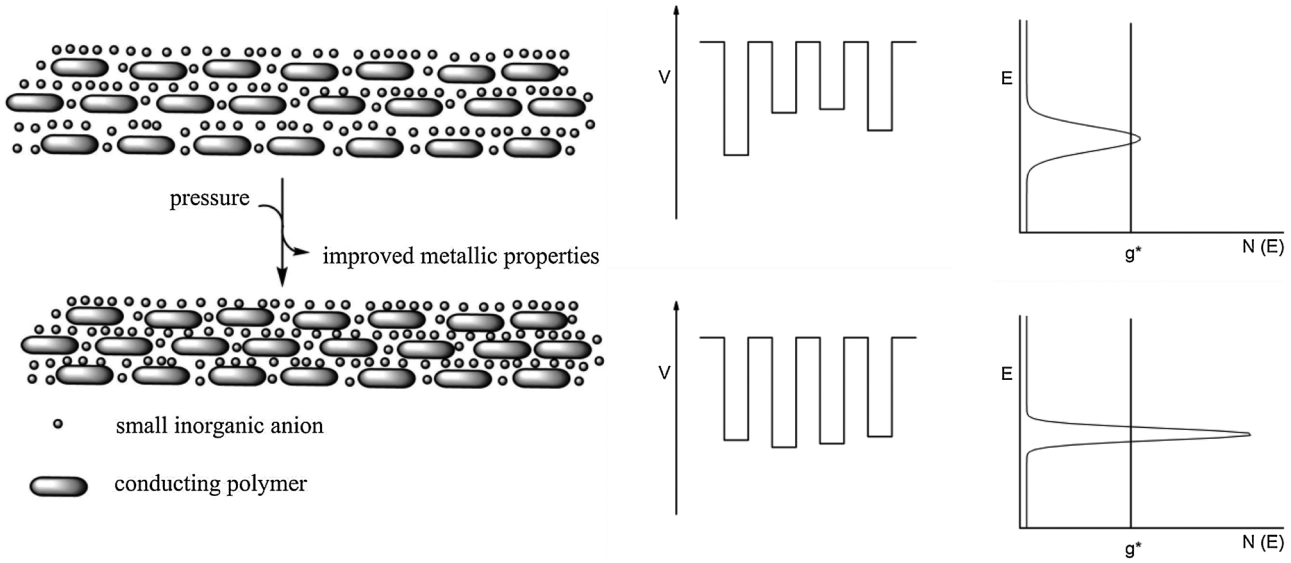

Fig. 1. Illustration of the effects of pressurizing PEDOT:sulphate. Without pressure (upper), structural order is already present, but the distances between the polymer chains are large, which results in a broader density of states. A metallic state (the g*-limit) is reached, but applying hydrostatic pressure may improve the material's performance (lower). Rising hydrostatic pressure induces denser packing, thus increasing the overlap between the wave functions of the polymer chains. This leads in turn to equalization of the hypothetical Bloch equations, and to electrons becoming able to move freely within the material as the mobility edge is transcended. It is highly likely that crystallites interact with their surroundings in a similar way.

Pressurizing the bulk specimen (~1000 nm) removes minor imperfections in the polycrystalline material, as it causes structural rearrangements that minimize disorder and thus narrow the distribution of states in the material [24,27].

A second effect of pressurization (which also applies to highly ordered systems, such as ours) is that increased packaging density promotes electron transport both between polymer chains and between crystal grains (see Fig. 1). This boosts the material's electrical performance, as diffusive electron transport is further enhanced. Hence, improved coherence among scattered charge carriers – as in a classical metallic conductor – is expected.

Due to the correlation between disorder and electrical performance mentioned above, structural characterization was paramount in this study. If conductivity depends mainly on local order, achieving crystallinity is critical to reach the metallic state. Hence, we conducted X-ray studies including specular X-Ray Diffraction (XRD) and X-Ray Reflectivity (XRR) to determine structural order in tandem with (magneto-)conductivity. We identified a strong relationship between the observed conductivity and structural order, and found single crystallites of sizes hitherto unreported in conductive polymers. Our findings are supported by results from Transmission Electron Microscopy (TEM).

1.1. Background and theory

Although inorganic (semi-)conductors differ intrinsically from their organic counterparts, many concepts, such as Anderson localization, have been accepted to be valid for both [28–33].

We characterized the structural properties of PEDOT:sulphate by XRR and XRD. In XRR, through observation of the position of the critical angle of total external reflection α_c, the electron density can be calculated from the formula

$$\alpha_C = \sqrt{2\delta} \tag{1}$$

where δ is the refractive index decrement used to calculate the refractive index n in the equation

$$n = 1-\delta + ic \tag{2}$$

and

$$\delta = \left(\lambda^2/2\pi\right) r_e \bullet \rho_e \tag{3}$$

where δ is the absorption index, λ the wavelength of the incident radiation, r_e the classical electron radius, and ρ_e the electron density.

Crystallite sizes in the films can be estimated from the full width at half maximum (FWHM, β) of the peaks observed in the XRD spectra. To this end, the Scherrer formula is applied:

$$\tau = 0.9 \bullet \lambda / \beta \bullet cos\theta \tag{4}$$

where τ is the average crystallite size, λ is the wavelength of the incident radiation, β is the FWHM of a selected Bragg peak, and θ is half of the scattering angle 2 θ. Unless further corrections are applied, the result obtained from this calculation presents the minimum crystal size to be expected.

Once the degree of disorder in the material under study is known, the electrical properties must be characterized. In conductive polymers, crucial questions to be answered typically concern the metal-insulator transition (MIT; specifically, on which side of it the material is located), the dimensionality of the conductor with respect to carrier transport, and the electron scattering processes involved [34–38].

A particularly useful tool for visualizing the MIT of an electrical conductor is the W- or Zabrodskiii-plot [30], in which the dimensionless parameter W is plotted against temperature, corresponding to Eq. (5).

$$W = -\frac{d\, ln\rho}{d\, lnT} \tag{5}$$

In such a plot, W (or, more precisely, its slope) allows distinguishing between a temperature-activated process in the critical regime of the MIT (W_T constant), a glassy metal just shy of the Mott-Ioffe-Regel (MIR) limit [39–42] ($W_T \ll 1$ and $W_T \propto T$), and a crystalline metal when the MIR limit is reached ($W_T < 0$ and $W \propto T$).

Beyond the temperature of the MIT, the correlation lengths of carriers become particularly interesting. A charge carrier's correlation length depends on various factors such as phonon-electron interactions, impurity scattering, and electron-electron interactions. These scattering processes are expected to change in character when lower temperatures are reached [43,44].

In conductive polymers (*i.e.* in disordered systems), these effects have been well described by Kaiser et al [13,45,46]. When carriers move through a disordered conductor, two scenarios will occur: at low temperatures elastic scattering processes will dominate, while at high temperatures inelastic scattering processes will. As in the case of the former (almost) no energy exchange between phonons and electrons occurs, the mobility of the carriers is dependent only on their intrinsic energy: localization occurs even on shallow traps and conductivity is thus low. In the case of the latter, exchange of energy between the "lattice" and the electrons occurs (emission or absorption of a phonon), helping the delocalization of carriers: conductivity is thus expected to rise, *i.e.* a negative temperature coefficient of resistivity (TCR) will be observed. This process is often referred to as weak localization.

The effects on conductivity are thus on the contrary of what is expected from a metal, where a positive TCR, *i.e.* an increase in conductivity upon cooling is expected. Concerning phonon scattering, an exponential dependence on temperature T is expected when $\ll \theta_D$, the Debye temperature, while a linear dependence is expected at $T \sim \theta_D$ [44].

Electron-scattering mechanisms can best be monitored by performing magnetoconductivity (MC) measurements. Varying the magnetic field at a fixed temperature affects a material's conductivity. In highly disordered conductive polymers, typically only magnetolocalization (*i.e.*, a decrease in σ *vs.* B) can be observed [47,48]. As the magnetic field is ramped, carriers become increasingly localized due to electron-electron interactions. In the rare case of metallic conductive polymers, however, an interplay between magnetolocalization and magnetoconductivity can be observed. Weak magnetic fields result in a resonance effect with the free carriers (due to weak localization), thus increasing the conductivity observed. At higher temperatures, this effect is thought to originate from weak localization. At high fields, weak localization is suppressed by electron-electron interactions increasingly resulting in magnetolocalization [23,34,37]. (Supporting Information, Fig. S1)

These positive and negative MCs are proportional to H^2 and $H^{1/2}$, respectively (Supporting Information, Fig. S2 and S3) [34].

If both localization and delocalization are present, the magnetic field can be reformulated to the magnetic penetration depth or the Landau orbit size L_D:

$$L_D = \sqrt{\frac{h}{e \bullet B}} \tag{6}$$

The resulting maximum then corresponds to the mean free path of charge carriers, $L_D \approx \lambda_e$, as the resonance condition is fulfilled.

A charge carrier's correlation length corresponds to various factors, such as phonon-electron interactions and electron-electron interactions. These processes, also referred to as scattering, is expected to change in character when lower temperatures are reached [7,13,43]. In a conductive polymer in the critical regime, a charge carrier is subject to inelastic scattering processes, and thus an inverse relationship between temperature and mean free path is expected. In the metallic regime, however, carriers are subject to elastic scattering processes, which allows scattering against the direction of carrier movement. At the transition from critical to metallic regime, a drop in the mean free path of carriers is therefore expected.

2. Experimental

Prepared by oCVD, all PEDOT:sulphate films were grown on glass and sapphire substrates. The synthesis is described in full detail elsewhere [23]. The growth time for micrometer-thick films was determined to be 1 hour for a 3 L/min carrier gas flow. Using a clean wooden toothpick to remove the film from the glass surface, we obtained mechanically stable, free-standing films.

For the samples used in XRD and XRR measurements, proportionally shorter growth times and flow rates of 1 L/min were used in order to obtain thin films with thicknesses of approximately 10 and 43 nm. Sapphire (0000) substrates served as carrier substrates.

Specular XRD and XRR data were collected on a PANalytical EMPYREAN diffractometer using Cu K_α radiation (λ = 1.54 Å). On the primary side, a parallel beam was generated using a multilayer X-ray mirror. On the secondary side, an anti-scatter slit and a Soller slit with a spacing of 0.02 rad were used with a PANalytical PIXcel^{3D} detector.

All conductivity measurements were performed using a Quantum Design-Dynacool PPMS system and the necessary (CuBe) pressure cell. This special alloys interaction with magnetic fields is minimal, allowing magneto-transport measurements. The sample is introduced to the cell in a pressurization-medium-filled teflon-cap and screwed shut. In order to apply a pressure load, a hydraulic press acting on a pressurization pin exerts pressure on the cells inside. Hence, the screwing cap can be further tightened, allowing measurements at elevated load pressures. (Fig. S4, SI)

For conductivity measurements, free-standing films of PEDOT:sulphate were mounted on a 4-probe sample board (4 in-line gold contacts, 1 mm separation) and inserted into the pressure cell. Daphne 7373 oil was used as pressurization medium. Silver paste was used to contact sample and sample board. This was sufficient to maintain stable contact over the whole temperature range (1.85–300 K). Magnetic fields of 0 to 9 T were applied at pressure loads of 0, 0.42, 1.28, 2.13, and 2.56 GPa.

All TEM measurements were performed using a JEOL JEM-2011. The bulk film was transferred to a copper grid as described above. All images presented in this publication were obtained using the same focus and a voltage of 100 kV.

3. Results and discussion

Since we hypothesized that excellent structural properties are a prerequisite for metallic transport properties, we decided to determine the structural aspects first. Both reflectivity and diffraction X-ray studies of films with a nominal thickness of ~ 43 nm (see Fig. 2) were conducted to investigate material parameters electron density, crystallite size, and preferred orientation with respect to the substrate. For this purpose, thin films of PEDOT:sulphate were grown on sapphire substrates.By means of XRR measurements, we first investigated the electron density in PEDOT:sulphate films (see Fig. 2a). In the measurement of PEDOT:sulphate, two critical angles of total external reflection (α_c) were observed. The critical angle of the substrate, the larger of the two in Fig. 2a, was determined by measuring the sapphire substrate alone and indicates – as expected – a higher electron density of the substrate compared to the film. The first critical angle then corresponds to the film and was observed at 0.195° in 2Θ. From this value the electron density of the PEDOT:sulphate film can be calculated as 543 nm^{-3} [23].

Additionally, the XRR measurements give information about film roughness. The steep decrease in intensity at angles above the critical angle and the absence of Kiessig fringes suggest a relatively rough film.

In specular XRD measurements probing the out-of-plane film structure (see Fig. 2b), we observed three sharp Bragg peaks corresponding to the PEDOT:sulphate film at 2Θ angles of 6.59, 19.80, and 23.74°, which correspond to *d*-spacings of 1.341, 0.448, and 0.375 nm, respectively. No further peaks from the film were observed at higher 2Θ angles. The other peaks visible in the XRD measurement of the film can be assigned to the sapphire substrate. The small number of peaks from the film suggests a preferred orientation of the crystallites with respect to the substrate; the positions of the peaks imply that the first and third peaks belong to the same peak series (*e.g.* the 001 and 003 reflections), where the peaks at 6.59° and 19.80° are respectively the first -order and the third-order reflection of the same series. This is a further indication that there is a strongly preferred orientation of the crystallites within the thin film. Since only few peaks are observed that correspond to the

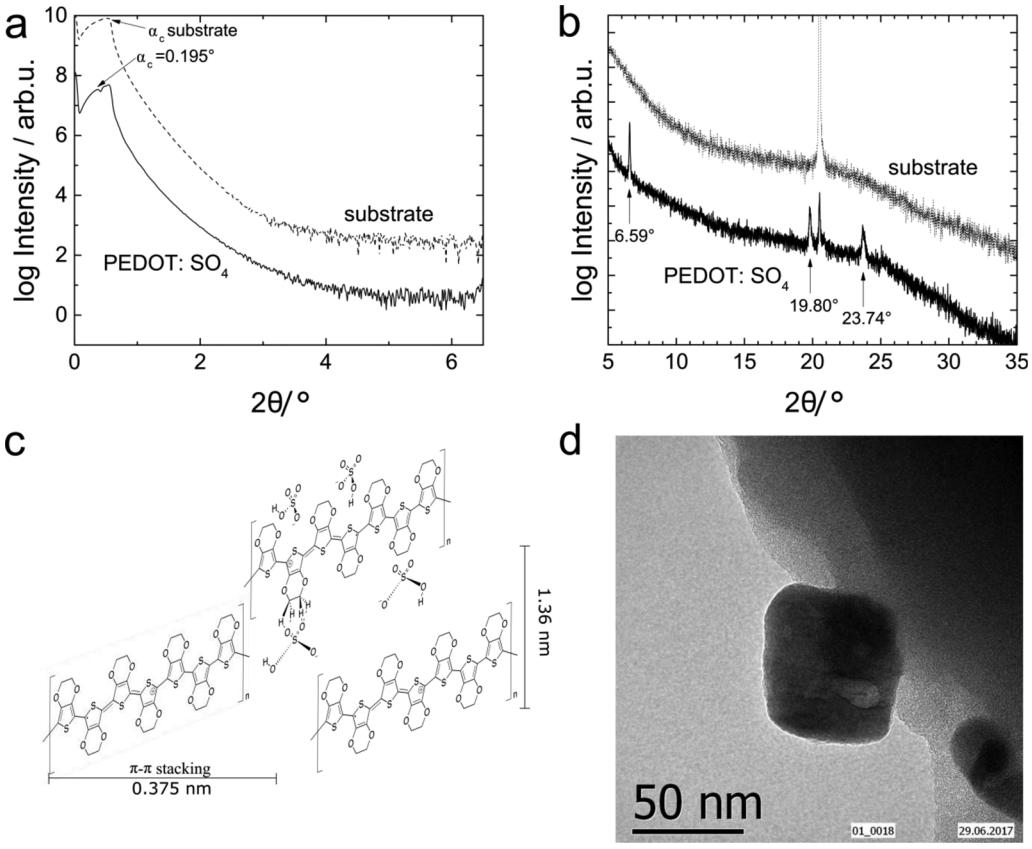

Fig. 2. Specular X-ray reflectivity and diffraction measurements. (a) Specular X-ray reflectivity curves of PEDOT:sulphate on sapphire (0000) and of pristine substrate. The critical angles α_c of both film and substrate are indicated. (b) Specular X-ray diffraction measurements of PEDOT:sulphate on sapphire compared with a measurement of the substrate alone. Peaks arising from the PEDOT:sulphate film are marked. (c) Schematic of the proposed packing in PEDOT:sulphate films. (d) TEM of a PEDOT:sulphate crystallite grain. The corresponding crystal diffraction pattern can be found in the SI (Fig. S2).

PEDOT:sulphate film no conclusions can be drawn about the crystal structure within the thin film, which - to the best of our knowledge- has not yet been published.

Based on the *d*-spacings observed, some information regarding the packing of the polymer chains can be made; a possible packing motif is shown in Fig. 2c. A layer spacing of 1.341 nm suggests that the majority of the polymer chains are standing upright on the substrate surface, as this *d*-spacing is of the same order of magnitude as the polymer chain length, accounting for the first two Bragg peaks. As specular XRD probes only the crystal structure perpendicular to the substrate, it yields no information about the in-plane crystal structure (parallel to the substrate surface). The Bragg peak at 23.74° (d = 0.375 nm) could correspond to a π-π interaction between neighbouring polymer chains. That this peak was observed in the out-of-plane direction means that polymer chains may also lie flat-on the substrate surface. Therefore, the polymer chains probably lie in two different orientations with respect to the substrate: one in which they stand upright (represented by the spacing of 1.341 nm and the higher order reflection) and a second in which they lie flat on the substrate surface such that the direction of the π-π interaction is in the out-of-plane direction (based on the *d*-spacing of 0.375 nm).

The specular XRD measurement can also provide information about approximate crystallite size in the out-of-plane direction. The FWHM of the first peak (2θ = 6.59°) suggests a crystallite size of ~ 80 nm perpendicular to the substrate surface, which dwarfs PEDOT crystallite sizes hitherto reported. Such a result highlights the high degree of order present in the films and explains the origin of the roughness encountered in XRR. In thin-films, a structure of islands (~ 80 nm) significantly larger than the nominal film thickness connected by thinner film areas (~ 43 nm) is present. Note that for the electrical measurements in this study the situation differed, as thick films (~ 1000 nm) exceeding the crystallite size were investigated. This structure of connected crystallites accords well with results obtained for other conductive polymers, but with an extraordinary degree of structural order [49–51]. In our case, these islands are essentially single crystalline grains; the XRD data available do not allow any conclusions to be drawn about the lateral crystallite size.

To gain a better understanding of the overall crystallite size, we performed TEM experiments and found crystallite sizes of up to 50 nm in thick films (see Fig. 2d, SI Fig. S5 which accords well with the results from XRD

At ambient pressure, the films exhibited a flat conductivity profile, retaining 52% of their room-temperature value even at low temperatures, specifically 2100 S cm^{-1} at 1.85 K (see Fig. 3a). In general, the conductivity plots in Fig. 3a indicate that two types of transport occur: temperature-independent band transport resembling that in a crystalline metal at low temperatures and temperature-activated transport resembling that in a disordered metal at elevated temperatures.

Further, compared to thin films, a new and important feature appeared in these measurements: a minimum in the conductivity value at 3.9 K (Fig. 3b), which corresponds to the minimum conductivity expected when the Fermi level approaches the mobility edge. This increase in conductivity is clearly attributed to the enhanced coherence in transport as electron-phonon scattering becomes weaker, and is a hallmark of the MIT (see Fig. 3c). Pressurizing the sample to 0.42 GPa shifted the minimum to 7.2 K. Upon gradual increase in pressure to 2.56 GPa, a further shift to 9.6 K was observed. At the same time, the material retained more of its room-temperature electron-transport properties at when pressurized, gradually approaching the flatter contour behaviour encountered in thin films, while the metallic minimum in conductivity became more pronounced (see Fig. 3d). This behaviour indicates an increasingly metallic character: increasing pressure improves the overlap between the wavefunctions of individual polymer chains and crystallite grains. We conclude that this effect is not caused by the samples Joule heating overcoming the systems cooling power. (see SI)

We were interested in observing the effects of a magnetic field on the transport properties. As both the minimum in conductivity and the

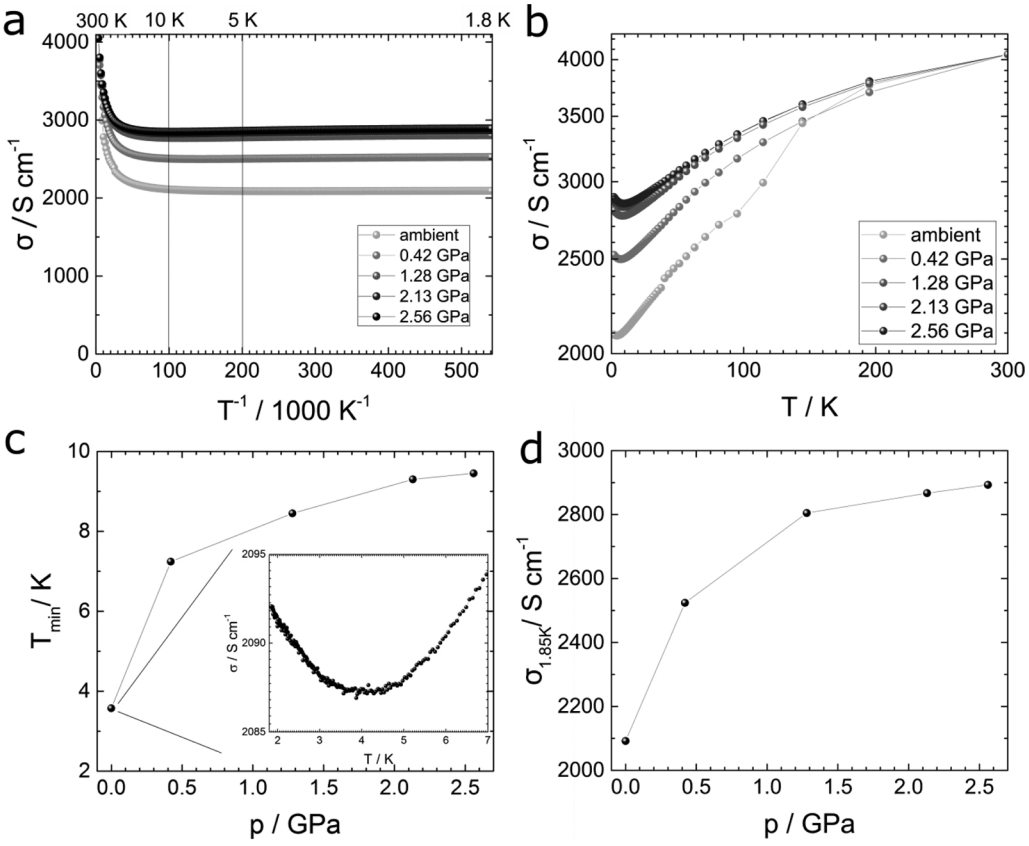

Fig. 3. Conductivity of PEDOT:sulphate free-standing films at various pressures at between 1.85 and 300 K. (a) Conductivity plotted against inverse temperature. The conductivity is comprised of two contributions: a temperature-activated transport term, which gradually diminishes with cooling, and a flat part corresponding to a metallic type of carrier transport. (b) Conductivity plotted against temperature. Note that the minimum in conductivity is found at temperatures below 10 K and shifts towards higher temperatures with increasing pressure, which points to a positive correlation between pressure and metallic character in PEDOT:sulphate. (c) Temperature at minimum conductivity under various pressures. The positive influence of higher pressure seems to approach a maximum to which T_{min} can be shifted. (d) Conductivity at 1.85 K for various pressures. As in the case of minimum conductivity, the positive effect of the applied pressure saturates.

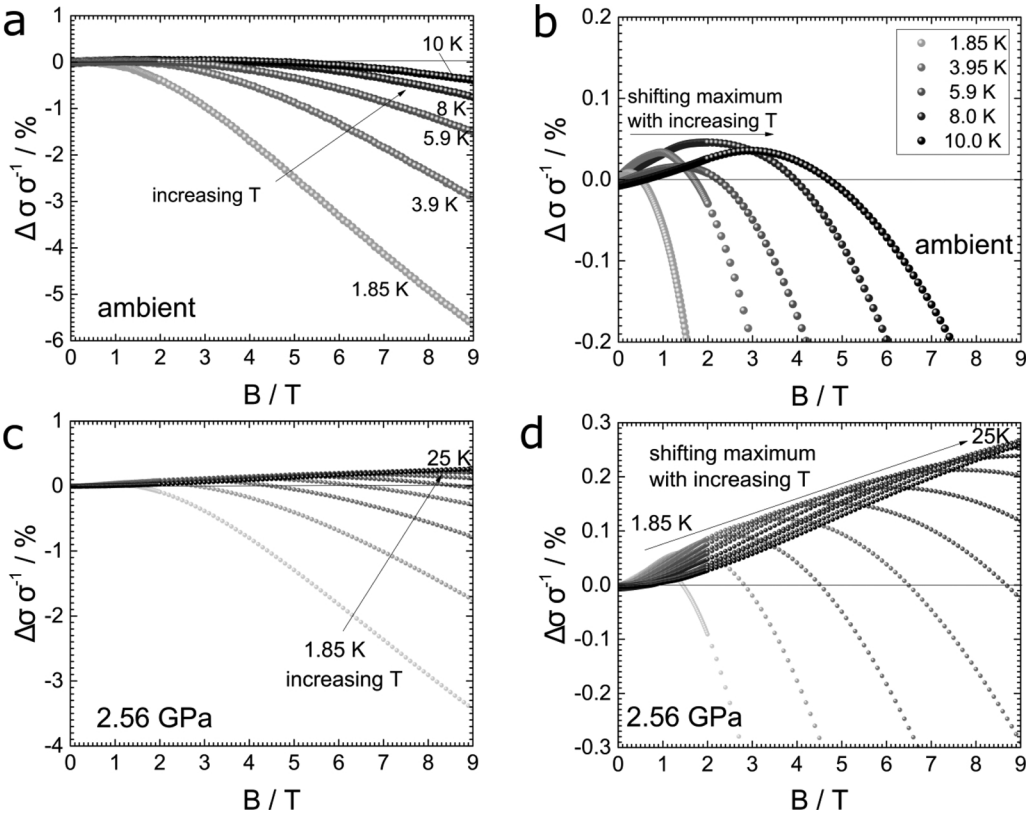

Fig. 4. Magnetoconductivity of PEDOT:sulphate at various temperatures and magnetic fields. (a) Magnetoconductivity (MC) change in percent at ambient pressures at temperatures between 1.85 and 10 K. (b) Enlarged version of Fig. 3a. The turning points at which destructive MC begins to dominate as a consequence of the strong magnetic field are clearly visible and manifest as a maximum. At higher temperatures, this maximum shifts to higher magnetic fields, as more energy is required to induce magnetolocalization. The positive effect was strongest at 8 K. (c) MC at 2.56 GPa pressure applied between 1.85 and 25 K (step size 2.31 K). (d) Enlarged version of Fig. 3c. The positive effect of the magnetic field on conductivity scales directly with temperature. As expected, a shift of the maximum to higher fields at higher temperatures was observed. Note that at temperatures above 20 K only positive MC was observed.

improved transport properties at higher pressures pointed to a material on the metallic side of the MIT, the question arose of how a magnetic field influences conductivity. In the case of a material on the metallic side of the MIT, interplay between positive and negative MC is to be expected. (see Fig. 4)

Subjecting the free-standing film to magnetic fields of 0–9 T at low temperatures resulted in the expected interplay (see Fig. 4a). The effect of magnetolocalization (*i.e.* negative MC) was most pronounced at 9 T and 1.8 K with a conductivity decrease of 5.8%. Higher temperatures, however, shifted the onset of magneto-localization to higher fields, with the positive MC becoming the dominant contribution (see Fig. 4b). This was most pronounced at a magnetic field of 2 T at 8 K, which resulted in a conductivity increase of 0.05%. Note that positive MC depends on B^2, whereas magnetolocalization shows a dependence on $B^{1/2}$ (for details see Figs. S2a and S3a, SI).

Upon pressurization, inter-grain and inter-chain transport improved, and the positive MC was further enhanced (see Fig. 4c). This is reflected by the maximum in MC shifting to higher magnetic fields with increasing temperature; at temperatures above 10 K, it was no longer possible to induce magnetolocalization (with the equipment available). Note that, upon exceeding 20 K, the positive MC effect was found to exceed 0.25% - an impressive value for a CP (see Fig. 4d) [52,53]. An evaluation of the magnitude of magnetolocalization can be found in the Supporting Information (see S2b and S3b, SI). Positive and destructive MCs showed the same relations to B as in the equivalent unpressurized setting.

We relied on MC to investigate the scattering mechanisms in the material, correlating them to metallic transport properties.

To this end, we reformulated the magnetic field strength B into the Landau orbit size L_D (Eq. (6); Fig. 5). At the maximum, the highest resonance between the magnetic field and the wave functions of the delocalized carriers is observed. This, we conclude, corresponds to the mean free path of electrons.

The results at ambient pressure (see Fig. 5a) indicate a hybrid scattering mechanism in PEDOT:sulphate films at minimum conductivity. While at temperatures of up to 3.9 K, a single resonance peak with a maximum scattering length of up to 49 nm (at 1.85 K) was found, the scattering length gradually decreased with temperature. At temperatures above 6 K, the maximum split, and a shoulder that indicates the coexistence of two scattering mechanisms appeared. We assume that this is caused by the difference in scattering within the crystallites and at the grain boundary. Higher temperatures diminish the two-phase resonance, thus enhancing that of shorter scattering length. We conclude that a phase transition from crystalline metallic to glassy metallic occurs in the two-phase regime, which is in agreement with the conclusions drawn from conductivity scans.

The coexistence of multiple resonances can be better understood when observing the MCs at elevated pressures (see Fig. 5b). Clearly resolved single peaks were observed when the elevated pressure fully masked the temperature effect (as previously observed), which supports our previous claim that increasing pressure increases the overlap between crystallite grains, thus favouring diffusive transport. Under pressure, the metallic phase established at higher temperatures, resulting in a scattering length of close to 40 nm, while the resonance value decreased gradually and arrived at 23 nm at 10 K. This is reminiscent of scattering theory stating that a transition from inelastic to elastic scattering leads to lower mean free paths as scattering becomes more coherent.

For better visualization, the collective results at different pressures applied are summarized in Fig. 5c and d. In general, higher temperatures resulted in shorter scattering lengths. When the sample was pressurized, a distinct change in behaviour was also clearly visible. The effect of increasing the pressure load saturated when approaching higher temperatures. Note that, irrespective of the level of pressure applied, scattering length approached a similar value with rising temperatures (see Fig. 5c).

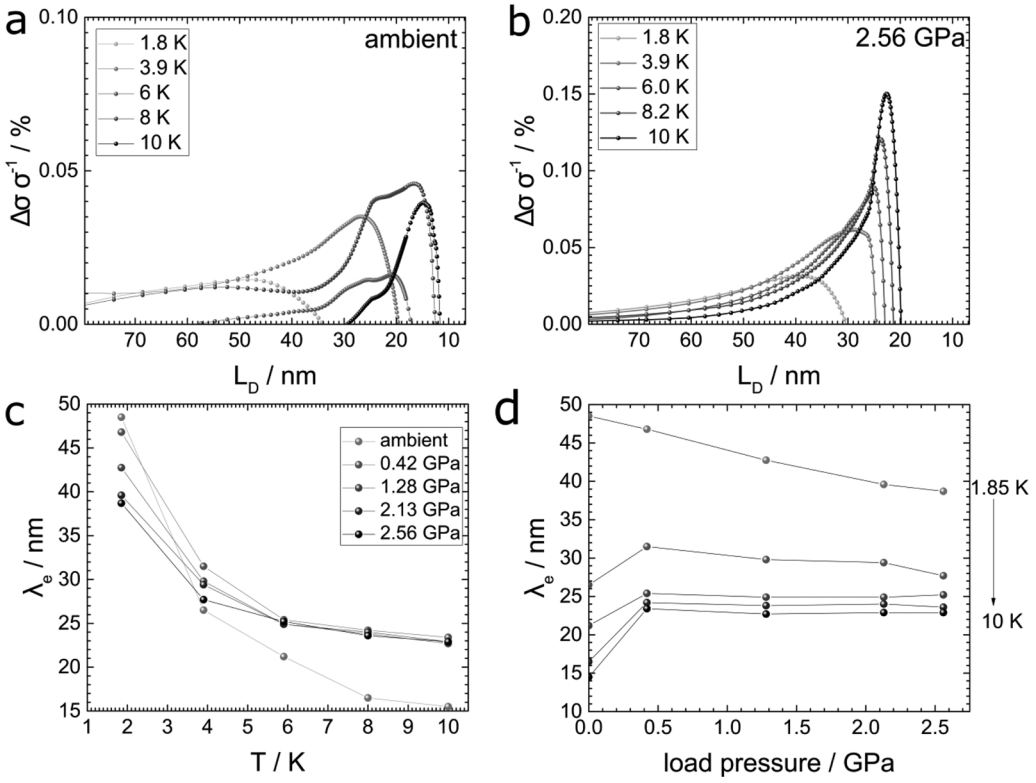

Fig. 5. Scattering lengths of free charge carriers at various pressures. (a) Landau orbit size or mean free path of carriers at various temperatures and ambient pressure. The maximum corresponds to a resonance of the magnetic field with conductivity. Note the shoulder above 6 K indicating a twin-resonance energy. This suggests the coexistence of elastic and inelastic scattering processes in the material. (b) Landau orbit size at various temperatures. The mean free path of carriers decreases with temperature. In contrast to the ambient pressure measurements, a single peak was observed, indicating the absence of a transition between scattering mechanisms. This trend was observed for any pressures applied (Supporting information, Fig. S7). (c) Correlation between mean free path of carriers and temperature. A common trend can be observed: higher temperatures correlate with a decrease in mean free path. This trend, however, is more pronounced in non-pressurized samples, as is to be expected. If pressurized, the mean free path decreases, approaching a value independent of pressure. (d) Correlation of mean free path of carriers with load pressure. For all pressures, at 1.85 K, elastic scattering and a linear decrease in mean free path can be observed. At higher temperatures, however, an interplay of two effects is visible: longer scattering lengths are increased by improved overlap between polymer chains and decreased by the transition from inelastic to elastic scattering. As the former effect saturates with pressure, an overall decrease in scattering length results.

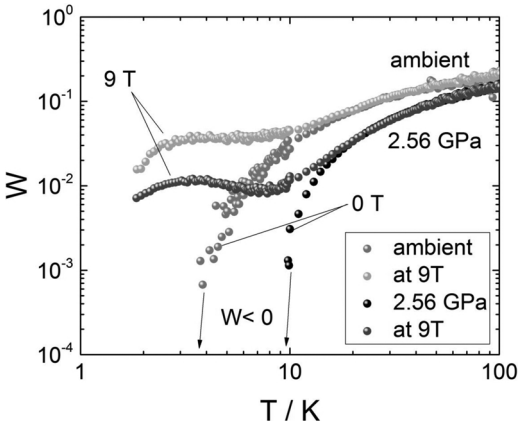

Fig. 6. W-plot and correlation between pressure and structural order. (a) W-plot at ambient pressure and at 2.56 GPa. In both cases, cooling the sample below 3.8 and 10 K, respectively, induced crystalline metal behaviour (*i.e.* a negative value of W), which correlates well with the expected behaviour. Elevated magnetic fields (9 T) quenched the metallic state to a certain degree and induced the critical regime of the MIT.

After an initial increase in mean free path upon pressurization (0.42 GPa), the effect of higher pressures on scattering length became limited (see Fig. 5d). This is a consequence of two competing phenomena occurring at the same time. On one hand, pressure improves the overlap between the polymer chains' wave functions, which increases conductivity and thus coherence among scattered electrons (see Figs. Figs. 2c and Figure 5d or SI Fig. S6). This "masks" the transition from inelastic to elastic scattering, where the improvement of the overlap is strongest. On the other hand, as scattering becomes increasingly elastic and the overlap approaches its optimum, the mean free path decreases in the expected way.

At 1.85 K, however, a decrease was observed regardless of the pressure applied, as the material was already on the metallic side of the MIT; elevated pressures immediately resulted in a drop in coherence length.

Finally, the data obtained from MC measurements allowed us to study the MIT in greater detail. We visualized the transitions between the various transport states in PEDOT:sulphate in the form of Zabrodskii- or W-plots (see Fig. 6). The effect of a strong magnetic field on the MIT was also investigated.

In the W-plots, measurements at ambient and elevated load pressures are quite distinct. In the absence of a magnetic field, the W-value of both decreases gradually upon cooling of the sample, as is to be expected of a glassy metal [23,34,52]. At some point, however, a transition towards the crystalline metal occurs as the W-value becomes negative. This happens when the sample's intrinsic conductivity starts to increase upon cooling, just as expected of a structurally ordered metal.

Upon applying a magnetic field of 9 T, the metallic properties become quenched in both cases, and the material enters a quasi-critical regime. Further cooling, however, gradually restores the behaviour of a glassy metal, as the destructive effects of the magnetic field are overcome.

The results constitute direct proof of our hypothesis that by significantly suppressing disorder, metallic properties can be induced in a polymeric conductor (see Fig. 1). The phenomenological gap (*i.e.* reaching a positive TCR) between inorganic and organic electrical conductors has been bridged, which shows that it is indeed possible to reach metallic properties in the absence of an elementary metal.

4. Conclusions

In bulk films of PEDOT:sulphate, charge carrier transport akin to that of a crystalline metal occurs due to a high degree of order. Hydrostatic pressure-induced shifts of the minimum conductivity σ_{min} show that anisotropic systems show transition from (weak) localization to metallic transport.

A look at magnetoconductivity reveals that the metallic regime exists readily at low temperatures. In particular, we observed a minimum at 3.9 K in highly crystalline CP samples. Furthermore, we have demonstrated that the crystalline-metallic regime can be expanded by elevated pressures, the effect saturating for higher pressures. Even relatively small pressures show significant effect. By raising the pressure to an extreme of 2.56 GPa, the MIT occurs already at 10 K, which represents a paradigm shift in conductive polymers.

Thus, we have confirmed that the metallic state depends on structural order and is well achievable in CP's. Expanding the metallic phase towards room temperature becomes thus the primary goal. We expect that achieving this in p-doped conductors will require chemically novel, yet simple, organic conductive materials.

Acknowledgements

P.S., N.S.S., and R.M. are grateful to OEAD (WTZ, IN10/2015). N.S.S. and D.F. acknowledge support from the Austrian Science Fund (FWF) within the Wittgenstein Prize scheme (Z222-N19 Solare Energieumwandlung) and the Austrian Research Promotion Agency (FFG; 842496, 3D OFET). The authors thank Markus Clark Scharber for fruitful discussions and Günter Hesser (Center for Surface and Nanoanalytics, Johannes Kepler University Linz) for TEM measurements.

Appendix A. Supplementary data

Supplementary material related to this article can be found, in the online version, at doi:https://doi.org/10.1016/j.synthmet.2018.03.015.

References

[1] M.N. Gueye, A. Carella, N. Massonnet, E. Yvenou, S. Brenet, J. Faure-Vincent, S. Pouget, F. Rieutord, H. Okuno, A. Benayad, R. Demadrille, J.P. Simonato, Structure and dopant engineering in PEDOT thin films: Practical tools for a dramatic conductivity enhancement, Chem. Mater. 28 (2016) 3462–3468, http://dx.doi.org/10.1021/acs.chemmater.6b01035.

[2] N. Massonnet, A. Carella, D.G. Arnaud, J. Faure-Vincent, J.-P.J.-P. Simonato, A. De Geyer, J. Faure-Vincent, A. de Geyer, J. Faure-Vincent, J.-P.J.-P. Simonato, Metallic behaviour in acid doped highly conductive polymers, Chem. Sci. 6 (2014) 412–417, http://dx.doi.org/10.1039/C4SC02463J.

[3] A. Ugur, F. Katmis, M. Li, L. Wu, Y. Zhu, K.K. Varanasi, K.K. Gleason, Low-dimensional conduction mechanisms in highly conductive and transparent conjugated polymers, Adv. Mater. 27 (2015) 4604–4610, http://dx.doi.org/10.1002/adma.201502340.

[4] N. Kim, B.H. Lee, D. Choi, G. Kim, H. Kim, J.R. Kim, J. Lee, Y.H. Kahng, K. Lee, Role of interchain coupling in the metallic state of conducting polymers, Phys. Rev. Lett. 109 (2012) 1–5, http://dx.doi.org/10.1103/PhysRevLett.109.106405.

[5] K. Lee, E.K. Miller, A.N. Aleshin, R. Menon, A.J. Heeger, J.H. Kim, C.O. Yoon, H. Lee, Nature of the metallic state in conducting polypyrrole, Adv. Mater. (Weinheim, Ger) 10 (1998) 456.

[6] O. Bubnova, Z.U. Khan, H. Wang, S. Braun, D.R. Evans, M. Fabretto, P. Hojati-Talemi, D. Dagnelund, J.-B. Arlin, Y.H. Geerts, S. Desbief, D.W. Breiby, J.W. Andreasen, R. Lazzaroni, W.M. Chen, I. Zozoulenko, M. Fahlman, P.J. Murphy, M. Berggren, X. Crispin, Semi-metallic polymers, Nat. Mater. 13 (2013) 190–194, http://dx.doi.org/10.1038/nmat3824.

[7] K. Kang, S. Watanabe, K. Broch, A. Sepe, A. Brown, I. Nasrallah, M. Nikolka, Z. Fei, M. Heeney, D. Matsumoto, K. Marumoto, H. Tanaka, S.I. Kuroda, H. Sirringhaus, 2D coherent charge transport in highly ordered conducting polymers doped by solid state diffusion, Nat. Mater. 15 (2016) 896–902, http://dx.doi.org/10.1038/nmat4634.

[8] J. Hynynen, D. Kiefer, L. Yu, R. Kroon, R. Munir, A. Amassian, M. Kemerink, C. Müller, Enhanced electrical conductivity of molecularly p-doped poly(3-hexylthiophene) through understanding the correlation with solid-state order, Macromolecules 50 (2017) 8140–8148, http://dx.doi.org/10.1021/acs.macromol.7b00968.

[9] A. Hamidi-Sakr, L. Biniek, J.L. Bantignies, D. Maurin, L. Herrmann, N. Leclerc, P. Lévêque, V. Vijayakumar, N. Zimmermann, M. Brinkmann, A versatile method to fabricate highly in-plane aligned conducting polymer films with anisotropic charge

transport and thermoelectric properties: the key role of Alkyl side chain layers on the doping mechanism, Adv. Funct. Mater. 27 (2017) 1–13, http://dx.doi.org/10.1002/adfm.201700173.
[10] A.B. Kaiser, Low-conductivity metals and comparison with highly conducting, Electron. Prop. Conjug. Polym. (1987), pp. 2–11.
[11] J.H. Mooij, Electrical conduction in concentrated disordered transition metal alloys, Phys. Status Solid 17 (1973) 521–530, http://dx.doi.org/10.1002/pssa.2210170217.
[12] A.B. Kaiser, V. Skákalová, Electronic conduction in polymers, carbon nanotubes and graphene, Chem. Soc. Rev. 40 (2011) 3786, http://dx.doi.org/10.1039/c0cs00103a.
[13] A.B. Kaiser, C.K. Subramaniam, B. Wessling, Electronic transport properties of conducting polymers, Int. Conf. Sci. Technol. Synth. Met. 64 (1994) 1–49 http://stacks.iop.org/0034-4885/64/i=1/a=201?key=crossref.95177e1e4908618ad4c8ee079a7a8b85.
[14] G. Bergmann, Weak localization in thin films: a time of flight experiment with conduction electrons, Phys. Rep. 107 (1984) 1.
[15] N.F. Mott, Metal-Insulator Transitions, 1st ed., Taylor & Francis LTD, London, 1974.
[16] N.F. Mott, Metal-insulator transition, Rev. Mod. Phys. 40 (1968) 677–683, http://dx.doi.org/10.1103/RevModPhys.40.677.
[17] N.F. Mott, Introductory talk; conduction in non-crystalline materials, J. Non. Cryst. Solids 8–10 (1972) 1–18, http://dx.doi.org/10.1016/0022-3093(72)90112-3.
[18] D. Belitz, T.R. Kirkpatrick, The Anderson-Mott transition, Rev. Mod. Phys. 66 (1994) 261–380, http://dx.doi.org/10.1103/RevModPhys.66.261.
[19] F. Evers, A.D. Mirlin, Anderson transitions, Rev. Mod. Phys. 80 (2008) 1355–1417, http://dx.doi.org/10.1103/RevModPhys.80.1355.
[20] A. Lagendijk, B. Van Tiggelen, D.S. Wiersma, Fifty years of Anderson localization, Phys. Today. 62 (2009) 24–29, http://dx.doi.org/10.1063/1.3206091.
[21] M. Imada, A. Fujimori, Y. Tokura, Metal-insulator transitions, Rev. Mod. Phys. 70 (1998) 1039–1263, http://dx.doi.org/10.1103/RevModPhys.70.1039.
[22] R.P. Fornari, P.W.M. Blom, A. Troisi, How Many Parameters Actually Affect the Mobility of Conjugated Polymers? Phys. Rev. Lett. 118 (2017) 86601, http://dx.doi.org/10.1103/PhysRevLett.118.086601.
[23] D. Farka, H. Coskun, J. Gasiorowski, C. Cobet, K. Hingerl, L.M. Uiberlacker, S. Hild, T. Greunz, D. Stifter, N.S. Sariciftci, R. Menon, W. Schoefberger, C.C. Mardare, A.W. Hassel, C. Schwarzinger, M.C. Scharber, P. Stadler, Anderson-Localization and the Mott-Ioffe-Regel Limit in Glassy-Metallic PEDOT, Adv. Drug Deliv. Rev. (2017), http://dx.doi.org/10.1002/aelm.201700050.
[24] K. Murata, K. Yokogawa, S. Arumugam, H. Yoshino, Pressure effect on organic conductors, Crystals. 2 (2012) 1460–1482, http://dx.doi.org/10.3390/cryst2041460.
[25] S.G. Duyker, V.K. Peterson, G.J. Kearley, A.J. Studer, C.J. Kepert, Extreme compressibility in LnFe(CN)6 coordination framework materials via molecular gears and torsion springs, Nat. Chem. 8 (2016) 270–275, http://dx.doi.org/10.1038/nchem.2431.
[26] E. Magos-Palasyuk, K.J. Fijalkowski, T. Palasyuk, Chemically driven negative linear compressibility in sodium amidoborane, Na(NH2BH3), Sci. Rep. 6 (2016) 28745, http://dx.doi.org/10.1038/srep28745.
[27] S.O. Dwyer, H. Xie, M. Knaapila, S. Guha, Conducting polymers under pressure : synchrotron x-ray determined structure and structure related properties of two forms of poly (octyl-thiophene), J. Phys. Condens. Matter. 10 (1998) 7145–7154 http://iopscience.iop.org/article/10.1088/0953-8984/10/32/006.
[28] N. Mott, Electrons in glass, Nobel Lect, Nature (1977).
[29] I. Solomon, Disordered semiconductors: The Mott-Anderson localization, J. Optoelectron. Adv. Mater. 4 (2002) 419–423 http://www.inoe.ro/JOAM/pdf4_3/Solomon.pdf.
[30] A.G. Zabrodskiii, K.N. Zinov'eva, Low-temperature conductivity and metal-insulator transition in compensate n-Ge, Zh. Eksp. Teor. Fiz. 86 (1984) 727–742.
[31] A.J. Heeger, N.S. Sariciftci, E.B. Namdas, Semiconducting and Metallic Polymers 21 Oxford Univ. Press, 2011, pp. 391–393, http://dx.doi.org/10.1007/s10904-011-9458-x.
[32] L. Torsi, M. Magliulo, K. Manoli, G. Palazzo, Organic field-effect transistor sensors: a tutorial review, Chem. Soc. Rev. 42 (2013) 8612, http://dx.doi.org/10.1039/c3cs60127g.
[33] H. Wang, U. Ail, R. Gabrielsson, M. Berggren, X. Crispin, Ionic seebeck effect in conducting polymers, Adv. Energy Mater. 5 (2015), http://dx.doi.org/10.1002/aenm.201500044.
[34] R. Menon, C.O. Yoon, D. Moses, A.J. Heeger, Y. Cao, Transport in polyaniline near the critical regime of the metal-insulator transition, Phys. Rev. B. 48 (1993) 17685–17694, http://dx.doi.org/10.1103/PhysRevB.48.17685.
[35] A. Aleshin, R. Kiebooms, R. Menon, A.J. Heeger, Electronic transport in doped poly (3,4-ethylenedioxythiophene) near the metal-insulator transition, Synth. Met. 90 (1997) 61–68, http://dx.doi.org/10.1016/S0379-6779(97)81227-1.
[36] K. Lee, S. Cho, S.H. Park, A.J. Heeger, C.-W. Lee, S. Lee, Metallic transport in polyaniline, Nature. 441 (2006) 65–68, http://dx.doi.org/10.1038/nature04705.
[37] P. Stadler, D. Farka, H. Coskun, E.D. Głowacki, C. Yumusak, L.M. Uiberlacker, S. Hild, L.N. Leonat, M.C. Scharber, P. Klapetek, R. Menon, N.S. Sariciftci, Local order drives the metallic state in PEDOT:PSS, J. Mater. Chem. C. 4 (2016) 6982–6987, http://dx.doi.org/10.1039/C6TC02129H.
[38] E. Helgren, K. Penney, M. Diefenbach, M. Longnickel, M. Wainwright, E. Walker, S. Al-Azzawi, H. Erhahon, J. Singley, Electrodynamics of the conducting polymer polyaniline on the insulating side of the metal-insulator transition, Phys. Rev. B - Condens. Matter Mater. Phys. 95 (2017) 1–8, http://dx.doi.org/10.1103/PhysRevB.95.125202.
[39] P.A. Lee, T.V. Ramakrishnan, Disordered electronic systems, Rev. Mod. Phys. 57 (1985) 287–337, http://dx.doi.org/10.1103/RevModPhys.57.287.
[40] C.C. Tsuei, Nonuniversality of the mooij correlationthe temperature coefficient of electrical resistivity of disordered metals, Phys. Rev. Lett. 57 (1986) 1943–1946, http://dx.doi.org/10.1103/PhysRevLett.57.1943.
[41] N.E. Hussey, K. Takenaka, H. Takagi, Universality of the Mott–Ioffe–Regel limit in metals, Philos. Mag. 84 (2004) 2847–2864, http://dx.doi.org/10.1080/14786430410001716944.
[42] M.I. Daunov, I.K. Kamilov, S.F. Gabibov, Concept of mobility threshold: The Ioffe-Regel rule, Phys. Solid State. 52 (2010) 2019–2025, http://dx.doi.org/10.1134/S1063783410100033.
[43] G. Bergmann, Physical interpretation of weak localization: A time-of-flight experiment with conduction electrons, Phys. Rev. B. 28 (1983) 2914–2920, http://dx.doi.org/10.1103/PhysRevB.28.2914.
[44] Ashcroft Mermin, Solid State Phys. (1976).
[45] A.B. Kaiser, Metallic behaviour in highly conducting polymers, Synth. Met. 45 (1991) 183–196, http://dx.doi.org/10.1016/0379-6779(91)91802-H.
[46] A.B. Kaiser, Systematic conductivity behavior in conducting polymers: Effects of heterogeneous disorder, Adv. Mater. 13 (2001) 927–941, http://dx.doi.org/10.1002/1521-4095(200107)13:12/13<927::AID-ADMA927>3.0.CO;2-B.
[47] M. Reghu, C.O. Yoon, D. Moses, P. Smith, A.J. Heeger, Y. Cao, Magnetoresistance in polyaniline networks near the percolation threshold, Synth. Met. 69 (1995) 271–272, http://dx.doi.org/10.1016/0379-6779(94)02446-6.
[48] A. Aleshin, R. Kiebooms, H. Yu, M. Levin, I. Shlimak, Conductivity and magnetoconductivity below 1 K in films of poly (3,4-ethylenedioxythiophene) doped with CF3SO3, Synth. Met. 94 (1998) 157–159.
[49] R. Noriega, J. Rivnay, K. Vandewal, F.P.V. Koch, N. Stingelin, P. Smith, M.F. Toney, A. Salleo, A general relationship between disorder, aggregation and charge transport in conjugated polymers, Nat. Mater. 12 (2013) 1038–1044, http://dx.doi.org/10.1038/nmat3722.
[50] C.G. Wu, S.S. Chang, Nanoscale measurements of conducting domains and current-voltage characteristics of chemically deposited polyaniline films, J. Phys. Chem. B. 109 (2005) 825–832, http://dx.doi.org/10.1021/jp046259b.
[51] S. Dongmin Kang, G. Jeffrey Snyder, Charge-transport model for conducting polymers, Nat. Mater. 1 (2016) 1–7, http://dx.doi.org/10.1038/nmat4784.
[52] R. Menon, Conductivity and magnetoconductance in iodine-doped polyacetylene, Synth. Met. 80 (1996) 223–229, http://dx.doi.org/10.1016/S0379-6779(96)03706-X.
[53] M. Ahlskog, M. Reghu, Magnetoconductivity in doped poly (p-phenylenevinylene), J. Phys. Condens. Matter. 101 (1998) 6779 http://iopscience.iop.org/0953-8984/10/4/012.